Additive Manufacturing 86 (2024) 104220

Contents lists available at ScienceDirect

Additive Manufacturing

journal homepage: www.elsevier.com/locate/addma

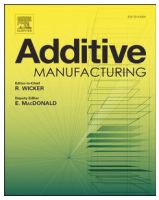

Two-photon polymerized wetting morphologies for tunable external and internal electrode micropatterning

Stanislav Sikulskyi [a,b], Rishikesh Srinivasaraghavan Govindarajan [a], Taylor Stark [a], Zefu Ren [a], Nicholas Reed [a], Daewon Kim [a,*]

[a] Department of Aerospace Engineering, Embry-Riddle Aeronautical University, Daytona Beach, FL 32114, USA
[b] Corning Incorporated, Painted Post, NY 14870, USA

ARTICLE INFO

Keywords:
Hydrophobic and hydrophilic
Two-photon polymerization (2PP)
Additive manufacturing (AM)
Electrode micropatterning
Microchannels

ABSTRACT

Numerous existing and emerging microsize technologies operate by utilizing electrical circuits on surfaces and within solid objects, i.e., external and internal electrodes, respectively. While current micropatterning techniques have achieved extensive progress on current systems via pattern resolution and discretization on simple surfaces, the introduction of new applications relies on the complexity of the parts on which these patterns are fabricated. Additionally, many state-of-the-art applications utilize novel materials for functional systems, which further complicates their fabrication. This paper introduces innovative electrode micropatterning and microchannel filling approaches that support complex 3D designs and reduce the number of fabrication steps. The approaches leverage microsize hydrophobic and hydrophilic morphologies fabricated using the two-photon polymerization (2PP) additive manufacturing (AM) process, in conjunction with the target part. Once fabricated, the part is dipped into a conductive solution or other functional liquids, forming patterns on the surfaces and filling the channels based on the pre-designed wetting morphologies. These morphologies incorporate additional structures beyond the conventional hydrophilic and reentrant hydrophobic structures to facilitate the dipping process. This paper demonstrates the efficacy of the tunable electrode micropatterning approach to fabricate various microsystems utilizing 2PP, wetting morphologies, and the developed dipping process.

1. Introduction

Emerging microsize technologies, such as microelectromechanical systems (MEMS), often require complex electrical circuits on their external and internal surfaces. Micropatterning electrodes for these technologies can be challenging due to small feature sizing, complex 3D structures, and unconventional materials. Currently, a number of approaches are being used to address this issue, including masked metal vapor deposition [1], laser ablation of precoated film [2,3], maskless jet printing [4,5], masked spraying [5], lithography [6], vacuum-based [7], capillary action driven [8,9], electrodeposition [10], and additive dispensing methods [11–13]. However, most of these techniques are tailored for particular geometry and scale, and thus, are spatially limited. Notably, only a single technique from the above demonstrated both internal and external electrode deposition, but consisted of several steps, utilized metal electrodes, and can be relatively sensitive to substrate scale and design [1]. Therefore, there exists a compelling need for an approach capable of micropatterning both external and internal electrodes with enhanced resolution, while not limited to flat horizontal surfaces. Additionally, this approach should be tunable to a multitude of intricate designs and electrode materials, while minimizing the need for numerous fabrication steps. This paper proposes and evaluates an approach to address the above challenges through leveraging two-photon polymerization (2PP) in producing wetting morphologies for electrode micropatterning via dipping. Namely, 2PP is used to fabricate the primary structure of a microsystem with its external and internal surfaces covered with a predefined pattern of wetting microstructures which either repel or attract liquids (Fig. 1a-1b). Once fabricated, the structure is dipped into a conductive solution (Fig. 1c). After dipping, the conductive solution remains on the predefined regions only and undergoes drying or curing, forming external and internal electrode micropatterns (Fig. 1c).

* Corresponding author.
E-mail address: kimd3c@erau.edu (D. Kim).

https://doi.org/10.1016/j.addma.2024.104220
Received 21 December 2023; Received in revised form 12 May 2024; Accepted 18 May 2024
Available online 22 May 2024

1.1. Wetting morphologies background

The influence of surface morphology on its interaction with various media has been actively studied for several decades, drawing significant inspiration from nature [14,15]. Wetting is amongst the most attractive properties of surface morphologies due to its promising performance enhancement, introduction of new functionalities, and its myriad applications [16,17]. Specifically, hydrophobicity and hydrophilicity are properties of a surface to repel or attract water, respectively. Hydrophobic microstructures utilize a liquid's surface tension to suspend it above the surface, thereby minimizing the wetted surface area and, thus, reducing surface free energy. As such, so-called reentrant structures have garnered significant attention for the ability to suspend liquids with low contact angles on surface materials, and for other hydrophobic capabilities despite their manufacturing complexity [18]. In contrast, hydrophilic morphology enhances surface free energy by increasing the wetted surface area [19,20]. While there has been tremendous success in altering the wettability of flat horizontal surfaces through the addition of fabricated microstructures, many advanced applications could be developed and benefit from the fabrication of wetting microstructures on variously oriented and curved surfaces [21,22]. However, manufacturing of complex high-performance microstructures is challenging. A variety of electrochemical techniques and processing procedures can be implemented but lack precise control, which is further complicated by intricate designs [23–26].

1.2. Two-photon polymerization (2PP) for wetting morphologies

To introduce new capabilities through wetting morphologies on intricate parts, this paper implements 2PP as the primary fabrication method. 2PP is a lithography technique that is capable of maskless 3D polymer structuring at sub-micron resolutions thanks to utilizing the two-photon absorption phenomena [27–29]. Therefore, 2PP can produce complex micro-scale components along with various wetting morphologies with high resolution in a single operation, drastically simplifying the fabrication process (Fig. 1a). The superior fabrication capabilities of 2PP have already been used to fabricate numerous designs of hydrophobic and hydrophilic microstructures [30–39]. Nevertheless, the above studies focus primarily on improving the performance of the wetting morphologies through complex microstructure design enabled by 2PP and 3D printed on flat horizontal surfaces. Meanwhile, as an AM technique, 2PP can enable fabrication of the microstructures on variously oriented and curved surfaces, and provide enhanced control and customization of the targeted wettability microstructure. Hence, the task of implementing 2PP for electrode micropatterning through the dipping process is to determine the limitations of 2PP fabricated microstructure complexity and size specifically for the proposed approach.

1.3. Development of micropatterning through dipping

Analysis of the dipping process and design of proper wetting microstructure is essential for the successful micropatterning of external and internal electrodes through the proposed approach. The dipping process fundamentally differs from most tests conducted with wetting microstructures, as the latter is mainly performed on horizontal surfaces. In contrast, known manufacturing methods that involve dipping often cater to parts with complex geometry that can be dipped in various orientations. Moreover, these parts are typically submerged in the solution fully rather than having individual droplets on the horizontal surface. This full immersion adds hydrostatic pressure to the Laplace and perturbation pressure components. Consequently, the dipping process is studied to investigate solid-liquid interaction and design of not only the primary but also the auxiliary wetting microstructures ensuring proper sequential contact between liquid and wetting morphologies on all surfaces as the part is dipped and pulled out. While the auxiliary microstructures are further introduced in the following sections, Fig. 1b-c illustrates three types of primary microstructures modified and designed in this paper to facilitate proper electrode micropatterning through dipping.

The first objective of the micropatterning approach addresses external electrode coating. The microstructure selected for this application is the simplest form of reentrant hydrophobic morphology that consists of a cylindrical stem and cap. Through analyzing the dipping process of vertical and horizontal surfaces, the reentrant microstructure design is adjusted for higher reliability and is accompanied by auxiliary microstructures to maintain wetting functionality. Furthermore, the practical limitations of 2PP for the proposed approach are studied. Lastly, the developed microstructure is utilized to fabricate a microsize strain gage, as shown in Fig. 1b1-c1.

The second objective of the micropatterning approach focuses on the internal electrodes inside the microchannels. As liquid electrode material comes in contact with the microchannel inlet, capillary action propels the material through the channel, with the limiting factors being

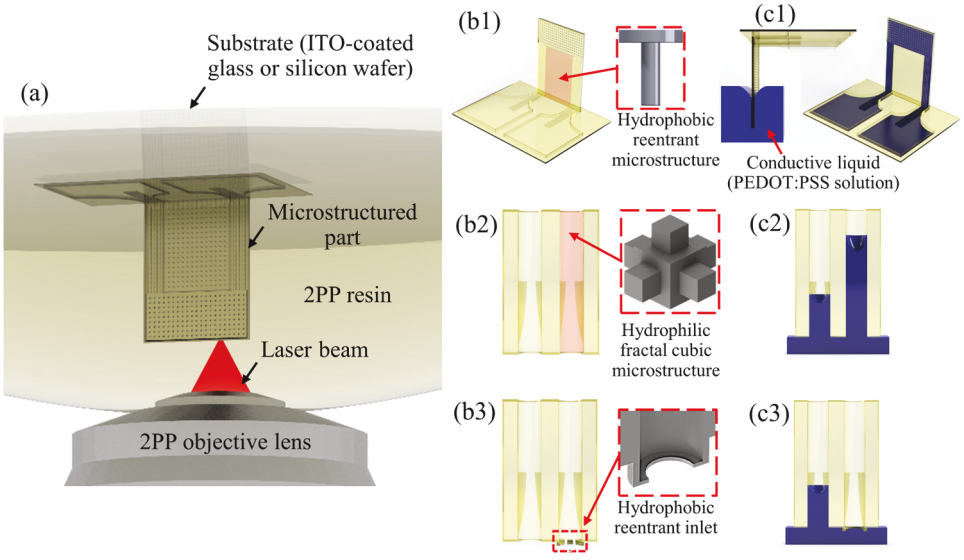

Fig. 1. Visual summary of the paper depicting (a) 2PP additively manufacturing small-scale objects with (b1-b2) hydrophobic and (b3) hydrophilic microstructures resulting in (c1) external electrode micropatterning, (c2) internal electrode filling, and (c3) selective microchannel filling or venting capability through dipping.

microchannel geometry and quality, and liquid surface tension and contact angle with the microchannel material [39–42]. Despite how channel wettability can be greatly enhanced as shown by microfluidics with hydrophilic structures [23,40], fabricating microstructures on the internal curved surface of a channel drastically restricts manufacturing options and possible microstructure designs. Typical methods utilize multiple open molds with pre-fabricated microstructures and subsequent assembly [41], resulting in structure misalignment, other defects, and reduced overall quality. Therefore, this work aims to additively manufacture channels with imprinted hydrophilic microstructures through 2PP. Highly hydrophilic fractal microstructures (Fig. 1b2-c2) with multiple overhanging features of various sizes, which have not yet been fabricated inside of microchannels to the authors' knowledge, are selected to demonstrate the capability of 2PP [34].

The third objective involves improving the patterning capability developed in the paper through the selective filling of the microchannels [41]. Hydrophobic structures at the inlet of a microchannel can prevent a liquid from entering the channel until a specific pressure is applied, as shown in Fig. 1b3-c3. Utilizing this approach offers several capabilities, such as leaving the microchannel empty for venting during one-sided electrode filling or selective microchannel filling with different liquids. Specifically, if a microdevice has multiple channels that require filling with different liquids, hydrophobic inlets can be placed on one end of each channel and tuned to suspend liquid on the respective ends [42].

2. Materials and methods

2.1. Materials

2PP resins: IP-S and IP-Q (Nanoscribe GmbH, Eggenstein-Leopoldshafen, Germany) resins are used for 3D printing structures with hydrophobic and hydrophilic microstructures, respectively. Different materials are used solely due to the different size scales of the microstructures and utilized printing lenses.

Propylene glycol monomethyl ether acetate (PGMEA) with 99.5 % concentration (Sigma-Aldrich Co., St. Louis, MO, USA, part #484431) is used to develop 2PP printed IP-S and IP-Q parts.

A surfactant-free 1.1 wt % aqueous solution of an intrinsically conductive polymer poly(3,4-ethylenedioxythiophene)poly(styrenes ulfonate) (PEDOT:PSS) (MilliporeSigma, Burlington, MA, USA, part #739332) is used for both the dipping process and filling the microstructured hydrophilic channels as an example of conductive solution for electrode coating due to its great application in various areas and the variety of commercially available aqueous solutions. The high content of water and absence of surfactants result in a water-like wetting behavior of the PEDOT:PSS solution, which simplifies its analysis and use with hydrophobic and hydrophilic structures.

A 1.3 wt % aqueous solution of an intrinsically conductive polymer PEDOT:PSS with 5 % surfactant (MilliporeSigma, Burlington, MA, USA, part #483095) is used for some tests with hydrophilic microstructures to evaluate their interaction with liquids possessing lower surface tension.

Surfactant plasticizer Triton X-100 ($C_{14}H_{22}O(C_2H_4O)_n$, where n=9–10) (Sigma-Aldrich Co., St. Louis, MO, USA, part #T8787) is added to PEDOT:PSS solution when electrode is used for the strain gauge experiment to reduce sensitivity of conductivity to low strains expected in the experiment and boost overall conductivity [43]. The materials are mixed such that the composition of the final electrode contained 20 wt % PEDOT:PSS and 80 wt % Triton X-100.

Isopropanol (IPA) (Duda Energy LLC, Decatur, AL, USA, part #isoprop), 99.9 % purity, is used for cleaning substrates, developing printed parts, and capillary testing of the microstructured hydrophilic channels due to its low surface tension.

Acetone (Duda Energy LLC, Decatur, AL, USA, part #acetone2), 99.5 % purity, is used for cleaning substrates before printing.

Polydimethylsiloxane (PDMS), Sylgard 184 (Dow Inc., Midland, MI, USA, part #4019862) is used for testing the microstructured hydrophilic channels.

2.2. Two-photon polymerization additive manufacturing

The fabrication of the hydrophobic and hydrophilic microstructures, along with the channels, is accomplished using a Nanoscribe Photonic Professional GT2 system (Nanoscribe GmbH, Eggenstein-Leopoldshafen, Germany) that is equipped with a 780 nm laser with a pulse duration between 80 and 100 fs and a repetition rate of 80 MHz. Hydrophobic structures are printed with IP-S, a highly viscous 2PP curable resin. All prints using IP-S resin utilize the 25x objective (0.8 numerical aperture) lens along with 1 in. x 1 in. indium tin oxide (ITO) coated soda lime glass substrates (MSE Supplies, Tucson, AZ, USA). For this configuration (25x, IP-S, ITO glass), standard printing parameters of 50 mW output power, 1.0 power scaling, slicing distances of 1 μm, hatching distance of 0.5 μm, galvo speed of 100 mm s^{-1}, and stitching angles equal to or greater than 15° are used to maintain mushrooms with no stitching effects. For better data and visuals, some of the parts are printed near the edge of the ITO coated glass substrates, while others are printed in the center of the substrates. The hydrophobic channels are printed with IP-Q resin on 1 in. x 1 in. silicon substrates utilizing the 10x objective (0.4 numerical aperture) lens. Standard printing parameters used for this configuration (10x, IP-Q, silicon substrate) are 45 mW output power, 1.0 power scaling, slicing distances of 5 μm, hatching distances of 1 μm, and stitching angle of 15°.

All printed parts, with the exception of the channels, are developed in PGMEA for 20 min, then in IPA for 5 min, and are blown dry with an airball. Due to the microchannels being filled with liquid resin during printing, to ensure the channels are fully developed, they are placed in PGMEA for 1 h at 70 °C, and then are placed in IPA for 10 min at 50 °C. The channels are then blown dry with an airball. The channels that appear to need more development are placed back in IPA and into a vacuum chamber set to 20 torr absolute pressure for less than a minute, to remove the air inside the channels while filling them with IPA. The parts are pulled out and left to sit in IPA for 10 min, and then are blown dry and inspected. If more development time is necessary, this process is repeated, applying sonication when needed.

2.3. Nanoindentation

Nanoindentation is performed to measure indentation hardness, H, and reduced modulus, E_r, later converted to Young's modulus, of the IP-S and IP-Q polymers using a Bruker Hysitron TI-980 TriboIndenter (Billercia, MA, USA). A force of 5 mN is applied to 300 μm diameter and 100 μm height cylindrical samples of IP-S and IP-Q with a 100 nm radius Berkovich diamond indenter prober. The measured reduced modulus and Poisson's ratio of 0.3 are used to calculate the Young's modulus of both the IP-S and IP-Q samples. Three segment indentation processes, including loading, unloading (1 mN s^{-1}), and a 5 sec dwell time, are executed as shown in Supporting Information Fig. S1. The measured values for both IP-Q and IP-S are listed in Supporting Information Table S1.

2.4. Microscopy and profilometry

A scanning electron microscope (SEM), the FEI Quanta 650 (Field Electron and Ion Company, Hillsboro, OR, USA), is used to assess the quality of the printed parts, and to investigate printing defects that could cause undesired wettability. The accelerating voltage of 10 kV is used for all the images. In addition, a Filmetrics Profilm3D (KLA Corporation, Milpitas, CA, USA), an optical profilometer with 10x and 50x Nikon objectives, is used to measure the thickness distribution of the deposited electrode.

3. Results and discussions

3.1. External electrode micropatterning through 2PP morphologies

This section presents the design of 3D printed reentrant hydrophobic microstructures, its testing results, and its application for an AM microsize strain gauge by controlling surface wettability to pattern electrodes.

3.1.1. Evaluation of 2PP for external micropatterning through hydrophobic microstructures

Hydrophobic behavior of reentrant microstructures, such as a mushroom-like design with a cylindrical stem and cap, on horizontal flat surfaces is a well-established phenomenon [15,21]. Maintaining the microstructures' spacing to be less than a liquid's capillary length allows the liquid to be suspended, as shown in Fig. 2a. Specifically, the liquid wets the top and side surfaces of the cap and remains suspended between the edges of the mushroom-design by its surface tension, γ, forming a suspended contact angle, θ, that varies due to the pressure difference, Δp, between the liquid and gas. If the pressure difference or the microstructure spacing is increased, the suspended contact angle would increase as shown in Fig. 2b. When the suspended contact angle reaches the Young's contact angle, θ_Y, of the liquid on the microstructure material, liquid propagates along the cap's bottom surface and stems to the base surface, transitioning from Cassie-Baxter to Wenzel wetting state as depicted in Fig. 2c-d, respectively. As illustrated in Fig. 2e, the liquid is supported by rectangular patterned microstructures while dipping. The sustained pressure can be obtained from the balance between the forces due to the external pressure and surface tension at liquid-solid edges. The maximum pressure threshold can be approximated with Eq. 1 when the suspended contact angle, θ, reaches the Young's contact angle, θ_Y.

$$\Delta p = p_L + p_h + p_p = \frac{\gamma \sin\theta \pi D}{\alpha^2 - \frac{\pi D^2}{4}} \tag{1}$$

where p_L is Laplace pressure, which is significant for small droplets, but has much smaller contribution when a liquid is spread more uniformly over a microstructured part during dipping; p_h is hydrostatic pressure, due to the depth of liquid, d_h, exerted on microstructures during dipping; p_p is perturbation pressure due to mechanical excitations of the microstructured part that are translated through the dipping apparatus and dynamic changes in environmental atmospheric pressure, etc.; D is cap diameter; α is the center-to-center spacing of the stems in a rectangular pattern.

For the successful implementation of the dipping process, several other factors need to be considered. Firstly, electrode liquid droplets should roll off the surface with hydrophobic microstructures upon the dipping, which corresponds to a small liquid hysteresis when on top of the hydrophobic microstructures. While an accurate prediction of hysteresis is complicated, a simple estimate of wettability can be obtained from the Cassie-Baxter model that describes the liquid's apparent angle, θ^*, as shown in Eq. 2.

$$\cos\theta^* = f_s \cos\theta_Y - f_g \tag{2}$$

where f_s is the solid fraction of contact with the liquid, i.e., the ratio of microstructures area in contact with the liquid to the projected area of the liquid-gas-microstructure contact, f_g is the gas fraction of contact with the liquid, i.e., the ratio of gas-liquid interface surface area to the projected area of the liquid-gas-microstructure contact. Because both horizontal and vertical surfaces of the reentrant microstructures wetted by the liquid and liquid-gas interface is curved between microstructures, the sum of solid and gas fractions are generally more than one, $f_s + f_g > 1$. Finally, θ_Y is the Young's contact angle between the liquid and the microstructures [21]. The usefulness of this relation for the developed dipping process lies in suggesting that the reentrant microstructures must result in a small solid fraction to facilitate liquid droplets rolling off the microstructured surface after dipping. The relation between the solid fraction, Young's and apparent contact angles as per Eq. 2 is illustrated well in literature [21]. In addition to minimizing the solid fraction of the designed hydrophobic microstructures, the surface roughness of the manufactured microstructures at the wetted area can be important [44,45].

Secondly, when liquid droplets do not completely roll off the surface, the effects of evaporation and consequent wetting must be considered. The transition from the Cassie-Baxter state to the Wenzel state during the droplet evaporation on horizontal microstructured hydrophobic surfaces has been studied with most common liquids, including water [46,47]. As the electrode liquid evaporates, the droplet size decreases and is supported by a smaller number of structures until it 'slides' between the structures, leaving undesired conductive areas on the base surface and hydrophobic structures, potentially compromising the electrode pattern functionality. One approach can be designing hydrophobic regions with enough microstructures to result in small residual droplets, and consequent conductive areas, between the conductive traces.

Finally, when the microstructures are used for patterning electrodes during the fabrication of a micro- or mesoscale device, it is ideal to minimize their effect on the device's geometry and functionality, which can be achieved by reducing the microstructure's size. Moreover, previous studies have reported the greater performance of smaller-scale microstructures [44,48]. Meanwhile, numerous experimental studies on reentrant hydrophobic microstructures show that these structures typically have morphology dimensions between 20 μm and 90 μm,

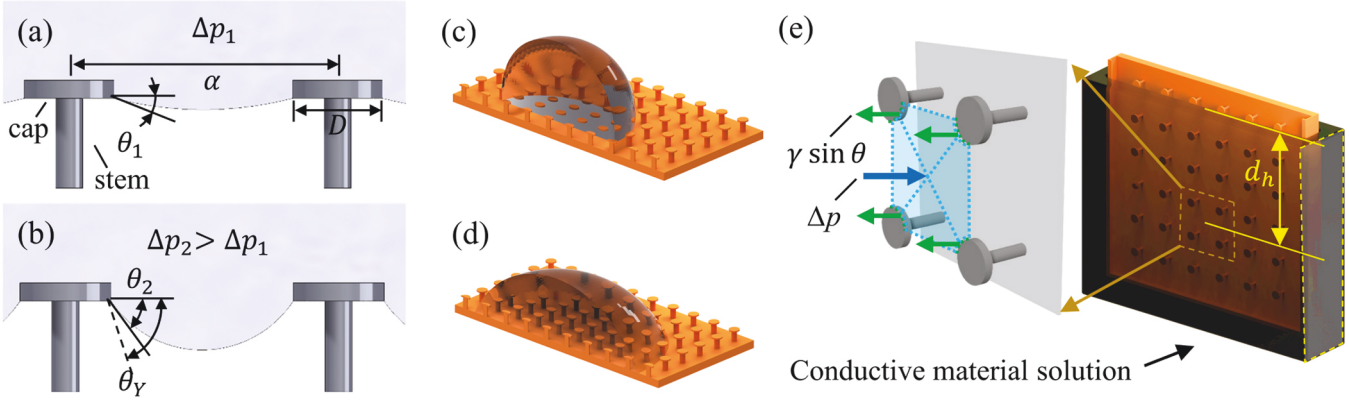

Fig. 2. Principle of reentrant hydrophobic microstructures (a) suspending a liquid at low pressure difference and (b) a higher pressure difference; (c) Cassie-Baxter and (d) Wenzel wetting states of liquid on a microstructured surface; (e) pressure equilibrium principle during the dipping process of a part with reentrant hydrophobic microstructures.

which is mainly limited by the utilized fabrication method [21,30,31,34,36,46]. Besides an obvious manufacturing resolution limitation, a fabrication method needs to be reliable in producing a large number of hydrophobic microstructures with a very high yield, as the failure of a single hydrophobic structure can lead to a complete failure of the hydrophobic layer and liquid propagating through the entire surface. AM of such miniaturized reentrant structures through the 2PP technique addresses both problems by enabling small-scale, high-quality features and replacing subtractive manufacturing with the additive process with its considerably lower chance of damaging the parts during fabrication.

To investigate and demonstrate the fabrication capabilities of 2PP for reentrant structure, a simple design of a former one is 2PP printed in a typical scale, then reduced to 1/3, and 1/6 size as shown in Fig. 3a-c. Fig. 3a demonstrates that the typical scale structures with the largest dimensions are printed with high fidelity on both the horizontal and vertical surfaces. The 1/3 design shows some deviation in shape between structures printed on the horizontal and vertical surfaces, as shown in Fig. 3b. The sizing of this design is selected close to the resolution of the 2PP printer 25x objective and, therefore, is modified by the software to enable successful manufacturing on horizontal and vertical surfaces with the 2PP printing voxel, which is an ellipsoidal shape with a high aspect ratio. The changes in the geometry can be observed in Table 1 and are used to evaluate the effectiveness of the scaled microstructures prior to dipping tests.

Firstly, the cap height of 1/3 scale design is increased in microstructures printed on the horizontal surface, but it only slightly increases the solid fraction, f_s, and, as a result, decreasing the apparent angle, θ^*, and increasing hysteresis, both to a small extent. Secondly, the 1/3 scale design is significantly affected by 2PP process in terms of the angle and its variation, independent of horizontal or vertical surface on which the mushrooms were fabricated (Fig. S3a). As the angle on cap bottom surface is the major factor determining the performance of reentrant hydrophobic microstructure, a statistical analysis was performed based on the dimensions of numerous 2PP printed mushrooms to ensure

Table 1
Dimensional measurements of 2PP printed reentrant hydrophobic microstructures used for investigating 2PP scale limitation and hydrophobic layer failure probability analysis. The shown standard deviations are based on measurements of 6–20 microstructures depending on the variability of the measured geometrical parameter.

	Surface	Angle on cap bottom surface	Cap overhang width [μm]	Cap width [μm]	Cap height [μm]
Baseline	Horizontal	5.4°±2.4°	9.5±0.2	28.9 ±0.6	9.6±0.2
	Vertical	6.6°±2.2°	7.3±0.2	25.5 ±1.0	6.7±0.4
1/3 scale	Horizontal	17.7°±8.4°	2.8±0.1	9.9±0.4	6.5±0.2
	Vertical	18.0°±8.7°	2.0±0.3	11.3 ±0.3	2.7±0.1
1/6 scale	Horizontal	n/a	n/a	n/a	n/a
	Vertical	n/a	n/a	n/a	n/a

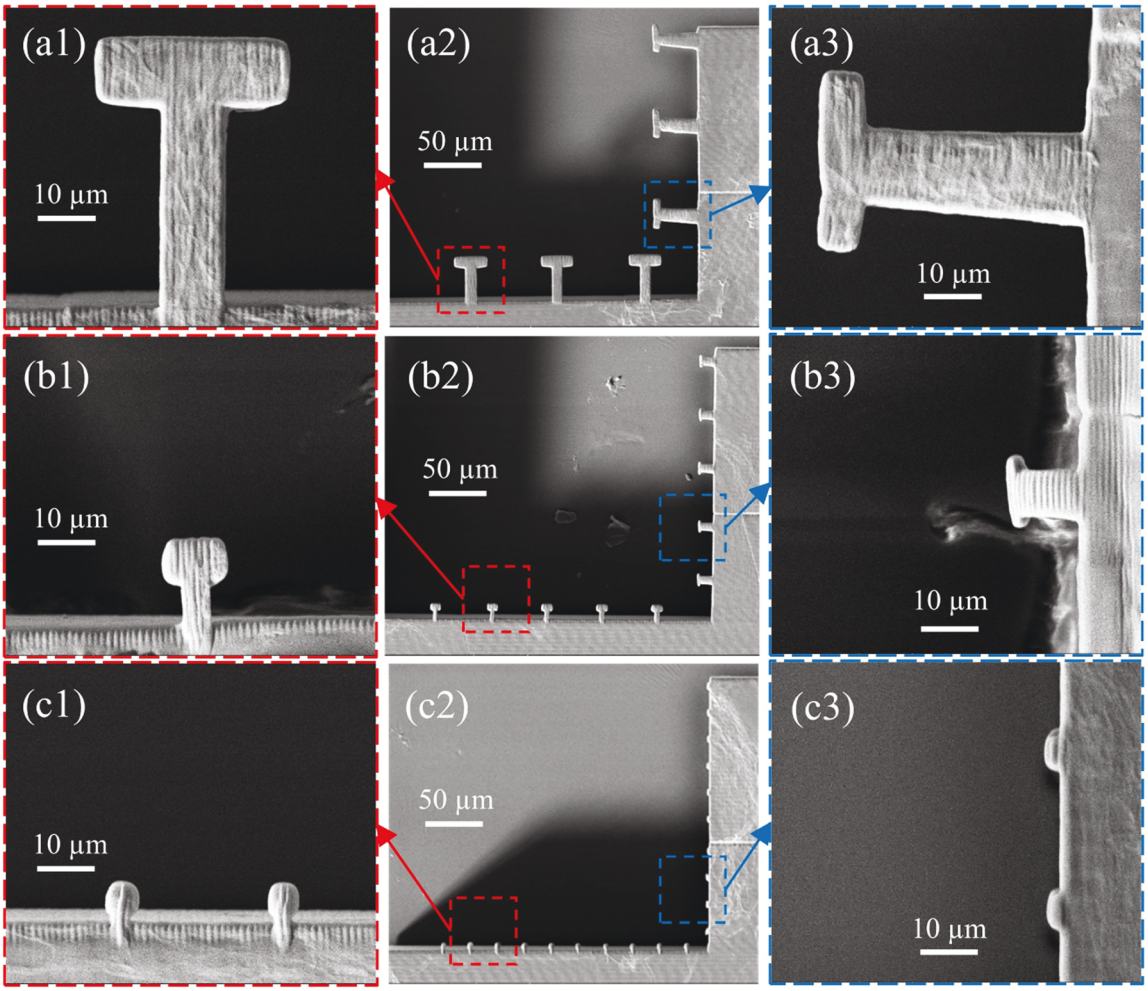

Fig. 3. Scanning electron microscopy of the cross-sections of reentrant microstructures additively manufactured with Nanoscribe GT2 2PP printer: (a1-a3) common sizing across literature, (b1-b3) one-third minimized size, and (c1-c3) one-sixth minimized size.

functionality. The probability density function (PDF) was plotted for the measured cap overhang angles of the mushroom on both horizontal and vertical surfaces together in Fig. 4a due to the angle values being statistically independent on the surface they were printed on (Supporting Information Fig. 3). The value of PDF at a given angle corresponds to a probability of the 1/3 scale mushroom design to have that angle on its cap overhang when fabricated through 2PP and being wetted by a liquid having a contact angle smaller than that. In Fig. 4a, contact angles of the 1.3 wt % PEDOT:PSS and surfactant-free 1.1 wt % PEDOT:PSS on IP-S are provided together with the corresponding PDF values. The analysis shows that the probability of a mushroom with 1/3 scale having the angle more than or equal to 58.9° and being wetted by the surfactant-free 1.1 wt % PEDOT:PSS is 3.51e-5 % (Fig. 4a). Fig. 4b demonstrates the failure probability of a hydrophobic area with numerous mushrooms assuming that the failure of a single mushroom results in the undesired electrode coating of the entire area. In this article, the structures with up to 2000 mushrooms have electrode coating failure probability of about 0.07 % due to the mushroom angle when dipped in surfactant-free 1.1 wt % PEDOT:PSS solution (Fig. 4b). Notably, a structure with 2000 mushrooms is guaranteed to fail when dipped into 1.3 wt % PEDOT:PSS solution, emphasizing the importance of the selected electrode liquid for successful micropatterning (Fig. 4b).

Regarding the rest of the geometry, cap width, cap overhang width, and stem height do not differ drastically between the horizontal and vertical surfaces and have small variation. However, it the decreased stem height in the 1/3 scale design does not leave much space for the curved liquid-gas interface that can cause a liquid contact with the base surface before the Young's contact angle is reached on the microstructure. Thus, the stem height is increased for this design in all further prints.

Finally, the structures shown in Fig. 3c are fabricated to identify the maximum capability of the objective and prove that the Fig. 3b design is the smallest possible implementation of the reentrant structure. Further minimization of the structure is possible when using a higher resolution objective, e.g., 63x lens (1.4 numerical aperture); however, it drastically increases the printing time of larger parts covered with microstructure. Hence, the reentrant microstructure design shown in Fig. 3b, but with increased stem height, is used for the rest of the fabricated and tested parts.

Furthermore, the performance of these three designs, in terms of the maximum liquid pressure that the microstructure can withstand, and the resulting apparent contact angle of droplets during their roll off after dipping is calculated through Eq. 1 and Eq. 2. These results are graphed in Fig. 5, conforming with the previous observations of higher performance with smaller microstructures. For calculations, the apparent contact angle of 1.1 wt % aqueous PEDOT:PSS solutions on IP-S 2PP printed flat surface is measured as 58.9°, as shown in Fig. S2 and

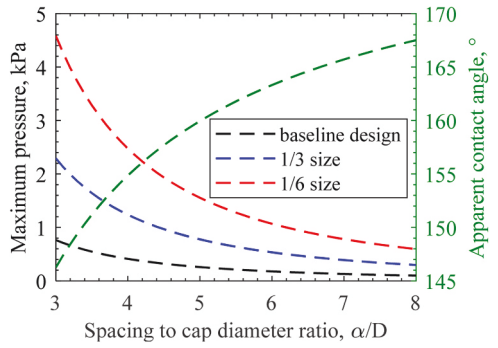

Fig. 5. Performance of three hydrophobic microstructure designs 2PP printed with IP-S resin in terms of maximum liquid pressure and apparent contact angle with surfactant-free aqueous PEDOT:PSS solution (98.9 wt % water). The baseline design represents the mushroom-like geometry with a cap diameter of 30 μm and a cap thickness of 6 μm. 1/3 and 1/6 size designs are proportionally miniaturized geometries, resulting in the same apparent contact angle for all three designs.

reported in Supporting Information Table S2. A water-like surface tension of 70 mN m^{-1} is used for the PEDOT:PSS solution as per literature [49].

3.1.2. *Integration of 2PP wetting morphologies for selective electrode coating*

This study aims to develop the wetting microstructure to pattern electrodes on parts of various geometries through the dipping process. Two samples with vertical and horizontal orientations of their base surfaces are first considered to investigate the wetting process during dipping. Testing setups, sample design features, and results are shown in Fig. 6 for the vertical and Fig. 7 for the horizontal samples. Both types of samples possess centrally located 0.5 mm×0.5 mm areas intended to be coated with electrode material through the dipping process that can be seen in Figs. 6a and 7b. These areas are either left with no morphology or covered with cones to investigate the effect of hydrophilic morphology on the dipping process (Fig. 6b1). The cones with equilateral triangle cross-sections and their sizing are selected to facilitate surface wetting and match the height of the hydrophobic structures. The remaining samples' area is covered with reentrant hydrophobic structures (Fig. 6b3).

The final vertical sample design, demonstrated in Fig. 6a, is further improved through experimentation and possesses a couple of modifications. The first vertical dip attempts demonstrated the inability of the utilized reentrant structures to support the liquid when it is fed sidewise to the microstructures. Therefore, vertical walls are added and further

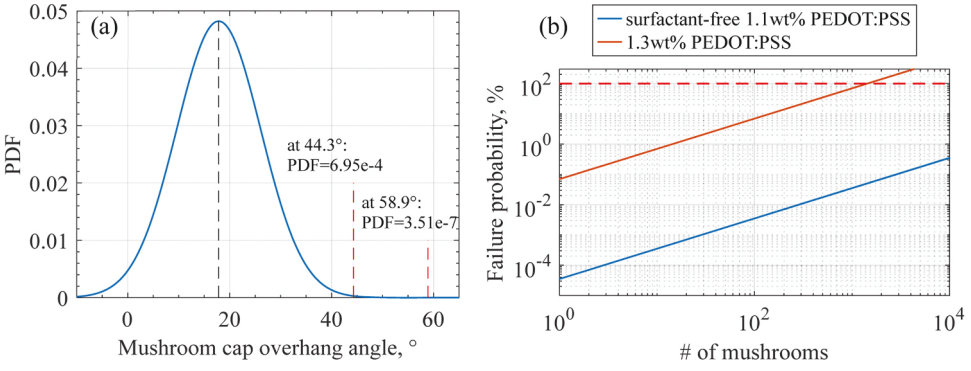

Fig. 4. (a) PDF of cap overhang angles for 1/3 scale mushroom design on both horizontal and vertical surfaces and shown contact angles of 1.1 wt % surfactant-free and 1.3 wt % PEDOT:PSS solutions on IP-S. The PDF values at those contact angles correspond to the failure probabilities of the mushroom design fabricated through 2PP with the given settings when in contact with the corresponding PEDOT:PSS solutions. (b) Failure probability of numerous mushrooms assuming that the failure of a single mushroom results in the overall failure of electrode coating with the surfactant-free 1.1 wt % PEDOT:PSS or surfactant-containing 1.3 wt % PEDOT:PSS.

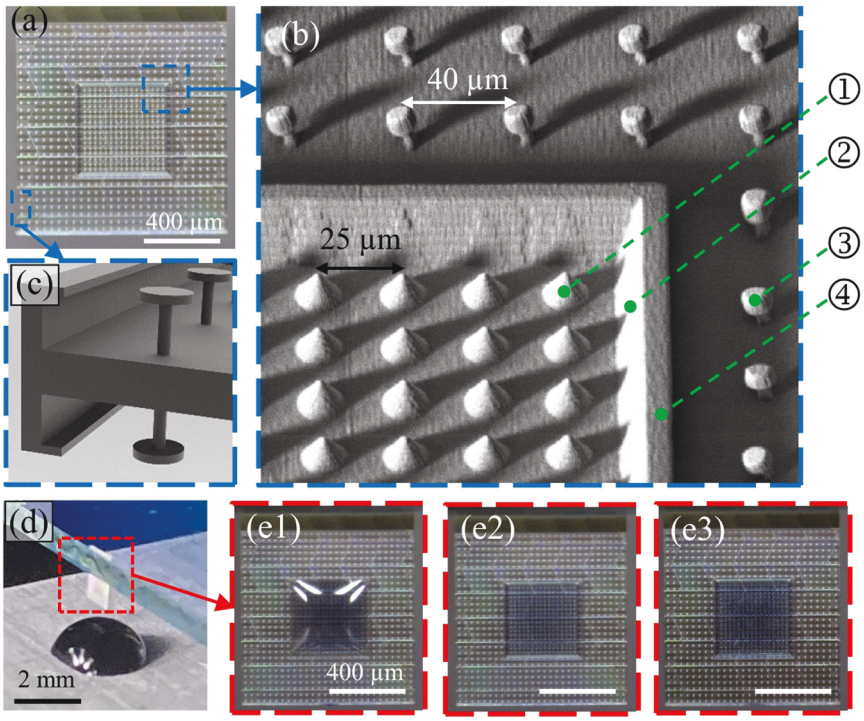

Fig. 6. (a) Front view of a sample for the vertical dipping test. The design consists of inner 0.5 mm×0.5 mm hydrophilic and outer hydrophobic areas. The microstructures include (b1) cones and (b2) the slope on the hydrophilic inner area, and (b3) hydrophobic reentrant structures (with the design as in Fig. 3b) encircled by inverted L-shaped edges on the (b4) inner and (c) cross-section of outer perimeters. (d) the vertical sample prepared for dipping in surfactant-free aqueous PEDOT:PSS solution (98.9 wt % water) and its close-up view after (e1) dipping, (e2) drying first layer, and (e3) drying second layer, demonstrating electrode deposition of controlled thickness on preselected region.

modified into inverted L-shapes to support the liquid on the edges of the hydrophilic region (Fig. 6b4) and the whole vertical sample (Fig. 6c), similarly to the individual reentrant structures. Lastly, Fig. 6d shows the dipping setup for the vertical structure and Fig. 6e1-e3 demonstrates the sample right after dipping it once, after drying the first coated layer, and after drying the second coated layer. The dynamics of coating multiple electrode layers on the vertical structure is also depicted in Supporting Information Movie 1. The PEDOT:PSS solution covers the hydrophilic area during the first dipping and also over the previously coated and dried layer. While successful coating is achieved, the dipping process unveils the importance of aligning the vertical structure with the PEDOT:PSS droplet to minimize the bending of the thin vertical structure and maintain correct wetting kinematics of microstructures. Furthermore, it is noticed that the vertical structures 2PP printed with IP-S bent less than samples made of IP-Q. This is attributed to the higher Young's modulus of IP-S polymer (3.396 ± 0.129 GPa) compared to the IP-Q polymer (1.488 ± 0.077 GPa), as measured with nanoindentation in Supporting Information Table S2 and Fig. S2.

Once the successful electrode coating through the dipping technique is achieved for the vertical sample, the dipping process is investigated on a horizontal sample with the same modifications as the vertical sample (Fig. 7a). Two hydrophilic areas, with and without cones, are fabricated on the surface to quantify the effect of the hydrophilic microstructure on the horizontal sample (Fig. 7b). First, the glass with the sample is placed above the PEDOT:PSS solution. Then, a substrate with the solution is raised until it touches most of the sample area (Fig. 7c1). Fig. 7c2 shows the horizontal sample right after the substrate with PEDOT:PSS solution is lowered. The dynamics of electrode coating on the horizontal structure are also depicted in Supporting Information Movie 2. The hydrophilic area with cones attracts considerably more solution than the area without any morphology. When analyzed through profilometry, the average thicknesses of the cured electrodes are approximately 1.35 μm and 0.73 μm for the areas with and without cones, respectively (Fig. 7d-e).

3.1.3. *Microsize strain gauge fabrication through 2PP wetting morphologies*

A microsize strain gauge with patterned electrode is fabricated through 2PP additive manufacturing and the developed dipping method, as shown in Fig. 8a, to validate its ability to coat electrodes for functional structures. The coating of the strain gauge electrode through the dipping process is depicted in Supporting Information Movie 3. The device's design is adapted from a conventional linear film strain gauge. However, it operates in a cantilever mode to sense its deformation due to the applied stimulus and is scaled down to 1.37 mm in height. Its principle of operation is through the change of resistance in the electrode coated on the surface of the vertical 2PP printed IP-S structure. Similar to the typical strain gauge, two large electrode connections were also coated away from the main structure to connect with multimeter probes. When the cantilever strain gauge bends, the electrode on the surface undergoes either tension or compression, depending on the bending direction. This affects its cross-sectional area and length, subsequently influencing the resistance. Fig. 8b shows the measured resistance gradually decreasing when up to 350 μm deflection is applied to the cantilever strain gauge, as shown in the experimental setup in Fig. 8c, which corresponds to about 0.8 % strain in the coated electrode layer.

3.2. *Internal electrode micropatterning*

Many applications utilize electrode micropatterns internally in the structure, which requires fabrication of microchannels and their enhanced and tunable filling process. This work aims to achieve the above requirements through 2PP printing of complex microchannels together with wetting microstructures on inside surface and at the channel inlets. Typically, fabricating complex microstructures on internal channels and other curved surfaces is challenging, especially when considering size and geometry constraints. These challenges can be addressed through multi-step fabrication processes but are still

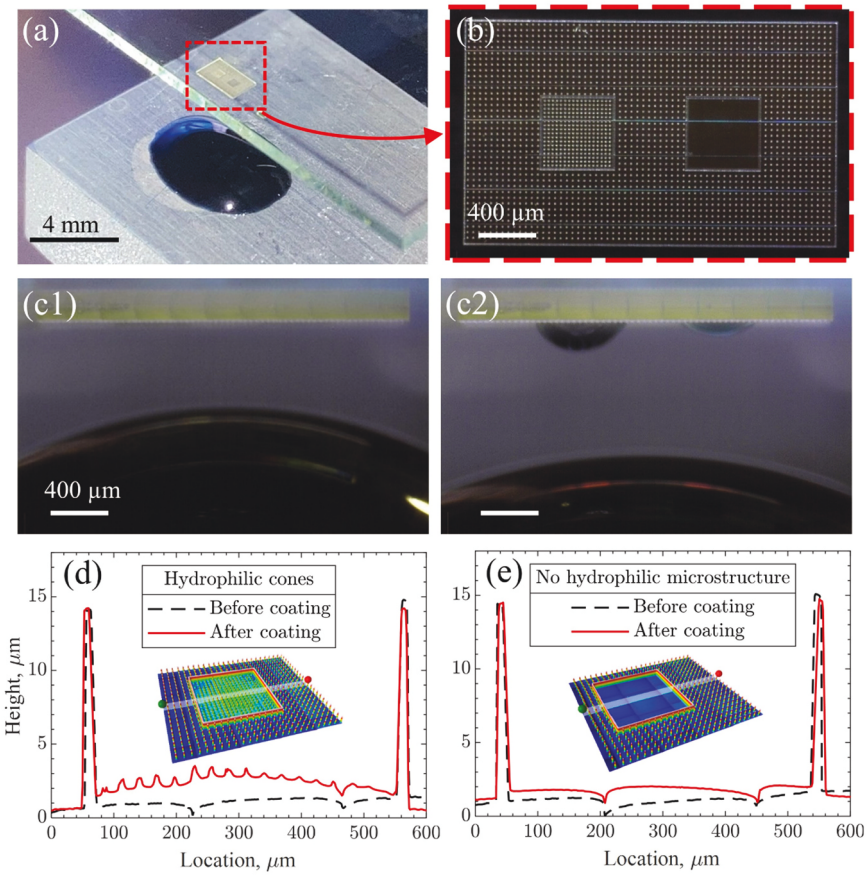

Fig. 7. (a) Horizontal sample prepared for dipping in surfactant-free aqueous PEDOT:PSS solution (98.9 wt % water) and (b) its close-up view. Two 0.5 mm×0.5 mm hydrophilic areas with and without conical morphology are located in the center of the sample. Side view of the sample (c1) before and (c2) after the dipping demonstrating a larger amount of material grabbed by the conical morphology. The thickness of the dried PEDOT:PSS electrode deposited on hydrophilic areas (d) with (1.35 μm average) and (e) without conical morphology (0.73 μm average).

limited in scope of application and microstructure design, such as complex fractals with overhanging features. To demonstrate the benefits of 2PP fabricated hydrophilic and hydrophobic electrode micropatterning for microscale channels, different microstructure patterns are designed and printed. Moreover, the third objective of this paper also serves to increase the tunability of the internal electrode micropatterning by providing a capability of selective microchannel patterning.

3.2.1. *Evaluation of 2PP for internal micropatterning*

The designed hydrophilic microstructures are cubic and pyramid fractal shapes with four layers of geometric patterning that are 2PP printed with testing structures, as shown in Fig. 9a-b, respectively. The pyramid fractal structure is designed to avoid overhanging features while the cubic fractal utilizes overhanging features extensively to increase the wetted area. Due to the absence of overhanging features in the pyramid structure, it is sought to be fabricable through other AM methods at a larger dimensional scale than presented in this paper.

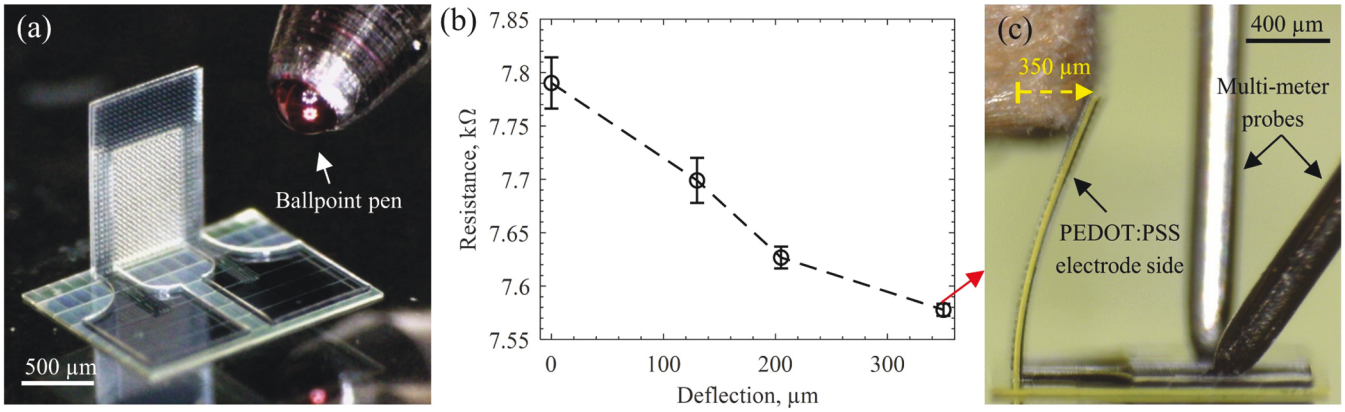

Fig. 8. Testing sensing capabilities of (a) 2PP printed microsize cantilever strain gauge structure and electrode pattern coated through the dipping technique (b) gradually decreasing resistance as the electrode is compressed (c) when deflected up to 350 μm that corresponds to about 0.8 % average strain in the coated PEDOT:PSS electrode at the root of the cantilever beam.

Meanwhile, the cubic structure possesses overhanging features, considerably complicating its manufacturing. A testing structure for measuring the change in capillary rise due to the effects of microstructure is also developed. A 4 mm long channel with a 3 mm diameter is patterned with microstructure, with a minimum feature size of 37.5 μm.

To determine the effect of the microstructure on the microchannel's wettability, an experiment is conducted to determine the change in capillary rise. For a cylindrical tube, the formula for capillary action is given by Eq. 3.

$$h = \frac{2\gamma\cos(\theta^*)}{\rho g r} \tag{3}$$

where h is the height of capillary rise, ρ is the liquid density, g is the gravity constant, and r is the radius of a cylindrical tube. Functionally, the addition of microstructure should minimally impact the surface tension of the liquid while drastically decreasing the contact angle, leading to an increase in the capillary rise. To determine this, microchannels are printed utilizing the 2PP printer, as described in Section 2.2. In addition to the patterned channels, a control channel is printed with no internal microstructure. The channels are then submerged in IPA liquid, and the depth of the meniscus is measured via microscopy, as shown in Fig. 10. In general, IPA has a lower surface tension compared to other common materials (mostly water or aqueous solutions, such as PEDOT:PSS). This reduces the amount of capillary rise, as well as the size of the channel required for the experiment, which makes printing more efficient and practical.

In the capillary rise tests with IPA, the complex cubic microstructure demonstrates the highest hydrophilic effect, with a 10.1 % increase in capillary effect over the smooth channel. The simpler pyramid microstructure also shows an increase, although less pronounced, at 4.3 %. Additionally, the effective contact angles for the IPA are calculated using the formula for capillary rise in a cylindrical channel using Eq. 3, and are listed in Table 2. This results in a 7.4° decrease in contact angle with the addition of cubic microstructure, and a 3.0° decrease in contact angle with the pyramid microstructure. These results match the general observations and assumptions about the effects of hydrophilic microstructures [35]. The increase in surface area provides a greater adhesive force with the sidewall of the channels, allowing for a greater capillary rise.

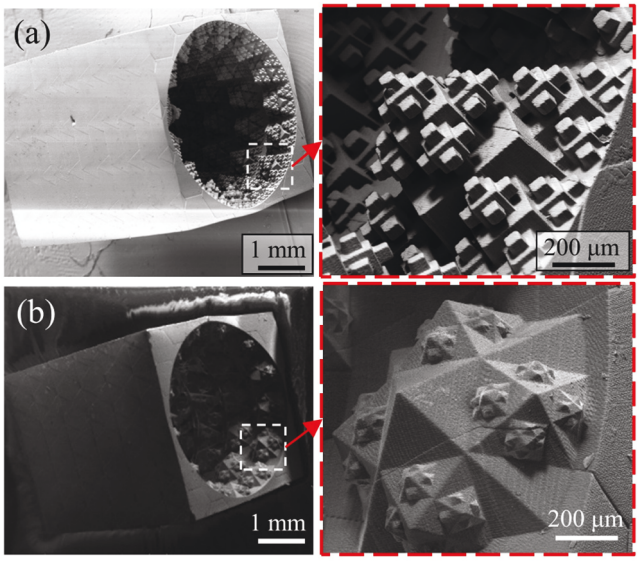

Fig. 9. SEM images depict 2PP microstructured channels, each lined on the inside with a complex fractal microstructure, with a minimum feature size of 37.5 μm. This allows for a significant increase in overall channel surface area. (a) The cubic microstructure offers more surface area than (b) the pyramid microstructure. Both are significant improvements over a smooth channel, with highly detailed, curved surface modifications that are difficult to achieve via other AM techniques.

Finally, to demonstrate the efficacy of microstructures in retaining more viscous polymers like PDMS, a comparison is performed between the best performing structure-augmented channel (cubic) and a smooth control channel. The 2PP printed channels are dipped into PDMS and allowed to fill via capillary action. The channels are then removed from the PDMS and allowed to drain, as shown in Fig. 11. The effectiveness of microstructured channels for that application is compared based on the height of the remaining liquid in the channels, h^*, measured after draining.

The PDMS testing results are shown in Table 3. Similar to the IPA testing, the capillary rise of the PDMS is greater in the microstructured channel than in the smooth channel. Notably, when removed from the PDMS, the patterned channel retains a large amount of PDMS below the edge of the structure ($h^{*'}$) that is still attached to the polymer initially pulled into the channel. This functionally increases the amount of PDMS present inside of the channel after the draining step, in comparison to the volume of polymer that flows into the channel via capillary action. However, the smooth control channel does not behave similarly and loses a large portion of the PDMS after draining. This test underscores the advantages of complex microstructures in filling and retaining low surface tension, high viscosity liquids, and polymers in microsize channels, making 2PP fabrication valuable in sensor applications where very viscous polymers, especially when mixed with sensing dopants and other chemicals, are used.

3.2.2. *Selective internal electrode micropatterning utilizing hydrophobic inlet*

The third objective involves coating electrode inside specific channels independently. Moreover, it can be desirable to have certain channels not filled with liquid or filled with a different liquid or polymer. Fig. 12a demonstrates how a hydrophobic microstructure consisting of a circular wall with an inverted L-shaped cross-section can be added at the inlet hole of a channel to prevent the microchannel from filling until a certain liquid pressure is reached. The maximum pressure the hydrophobic inlet can withstand is obtained from the force balance as shown in Eq. 4, when the contact angle, θ, approaches the Young's contact angle, θ_Y. Fig. 12a relates the maximum pressure that can be withstood by the inlet to its diameter, when dipped in different liquids. Thus, the inlet can potentially be used to fill several channels with various liquids controlled by the pressure that the hydrophobic microstructure is tailored to withstand. To experimentally demonstrate the effectiveness of 2PP in fabricating such structures, a system of helical microfluidic channels with a diameter of 400 μm, one of which features the hydrophobic inlet with a diameter of 300 μm, is 2PP printed with IP-S resin and is demonstrated in Fig. 12b. This system is then dipped into PEDOT:PSS solution to fill the channels. The regular inlet cannot resist the capillary effect, and the channel fills as depicted in Fig. 12c. The inlet with the hydrophobic microstructure prevents liquid from entering the channel, and can serve as a venting channel. Furthermore, the hydrophobic microstructure is able to resist hydrostatic pressure up to the point when half of the structure (about 2 mm) is dipped into the PEDOT:PSS solution. According to Eq. 4, the printed design should withstand about 0.8 kPa of liquid pressure, which corresponds to the hydrostatic pressure at 8.15 mm depth of surfactant-free aqueous PEDOT:PSS solution. This suggests that dynamic perturbations during dipping might considerably contribute to the liquid pressure. However, the exact impact of perturbation is hard to evaluate, as hydrophobic performance is also affected by the quality of the printed structure, which is not optimized for this inlet.

$$\Delta p = \frac{\gamma\sin\theta\pi D_i}{\pi D_i^2/4} = \frac{4\gamma\sin\theta}{D_i} \tag{4}$$

where D_i is the diameter of the hydrophobic inlet and the rest of the

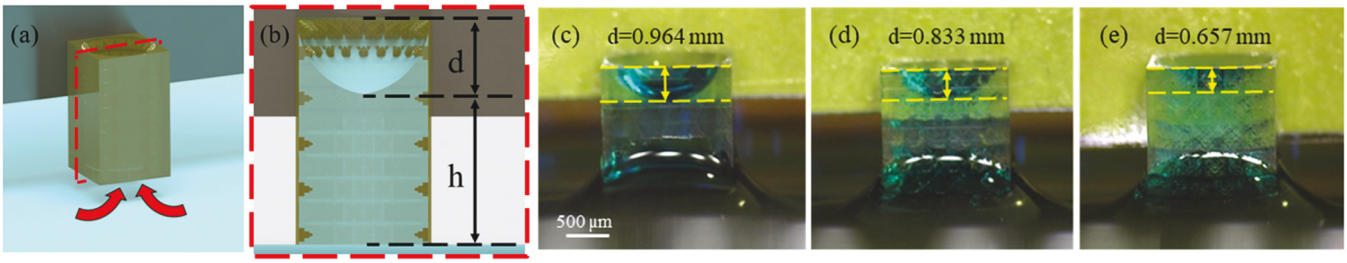

Fig. 10. (a) Experimental setup for the liquid dip testing. The 2PP printed channel is suspended over testing liquid, and is brought into contact with the surface, causing capillary action to pull liquid into the channel. (b) The capillary height is measured with respect to the top of the channel and the meniscus, since determining the exact location of the edge in the testing liquid is challenging. The liquid dip testing demonstrates the meniscus depth inside (c) smooth, (d) pyramid, and (e) cubic channels when immersed in IPA. The IPA is dyed blue to increase visibility. The structured channels show a significantly larger capillary rise compared to a smooth channel, which decreases the height from the meniscus to the top of the channel. Increasing the surface area by modifying the microstructure design similarly increases capillary rise further.

Table 2
Testing results of IPA capillary rise in microstructured channels and calculated contact angles.

	Meniscus depth [mm]	Capillary rise [mm]	Contact angle
Smooth	0.964	3.04	40.5°
Pyramid	0.833	3.17	37.5°
Cubic	0.657	3.34	33.1°

variables same are the same as in Eq. 1.

4. Conclusions

This paper demonstrates successful electrode patterning, on-demand and enhanced microchannel filling utilizing 2PP AM, and the design of wetting morphologies. Primary and auxiliary hydrophobic and hydrophilic microstructures were designed and fabricated through the 2PP process on variously oriented external and internal surfaces, resulting in programmable wettability for electrode coating through the dipping technique. Analytical analysis estimated that liquid pressure on the order of several kPa that can be withstood by hydrophobic microstructures of a typical geometry, suggesting that dipping is not limited by hydrostatic pressure for the size of parts that can be manufactured through 2PP. The effectiveness of the method for electrode patterning was first studied on vertical and horizontal external surfaces by selectively coating microsize areas with the electrode material. It was then used to demonstrate fabrication simplicity with an example of a functional microsize strain gauge, tested in the cantilever mode. The efficiency of the hydrophilic microchannels' morphologies was further evaluated by conducting the capillary rise test with various liquids. A new capability of the hydrophobic inlet was also designed and demonstrated for microchannels venting and selective filling. Future work of this study could focus on the design and fabrication of microsize devices that can drastically enhance their performance through the implementation of complex geometries and patterning methods enabled by 2PP and wetting morphologies.

CRediT authorship contribution statement

Taylor Stark: Writing – review & editing, Writing – original draft, Visualization, Validation, Software, Methodology, Investigation, Formal analysis, Data curation, Conceptualization. **Zefu Ren:** Writing – review & editing, Writing – original draft, Visualization, Validation, Software, Methodology, Investigation, Formal analysis, Conceptualization. **Stanislav Sikulskyi:** Writing – review & editing, Writing – original draft, Visualization, Validation, Software, Project administration, Methodology, Investigation, Formal analysis, Data curation, Conceptualization. **Rishikesh Srinivasaraghavan Govindarajan:** Writing – review & editing, Writing – original draft, Visualization, Validation, Software, Project administration, Methodology, Investigation, Formal analysis,

Table 3
Testing results of capillary rise and retained height of PDMS in microstructured channels.

	Height [mm]	Height retained [mm]
Smooth	1.83	1.54
Cubic	2.14	0.67 (2.08)

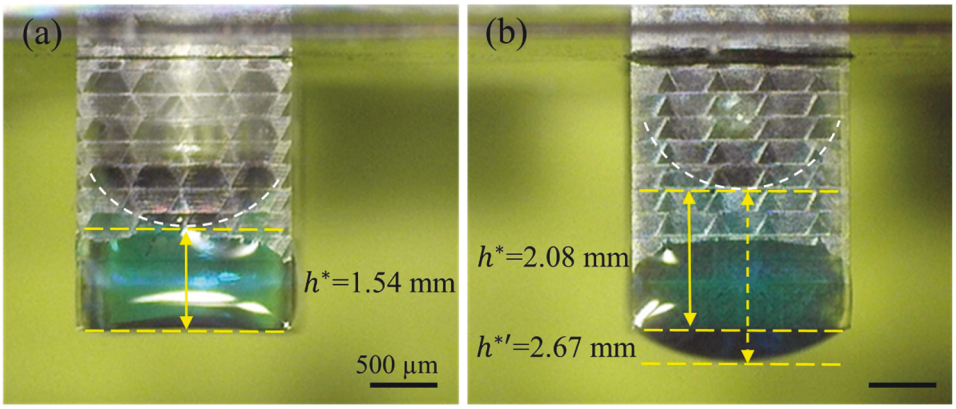

Fig. 11. Liquid dip testing demonstrating the meniscus depth for (a) smooth and (b) cubic channels after being dipped in PDMS, removed, and allowed to drain. The cubic channel retains significantly more PDMS than the smooth channel due to increased surface area. Additionally, the cubic structured channel retains additional PDMS beyond the edge of the channel, further demonstrating the increased capillary efficacy.

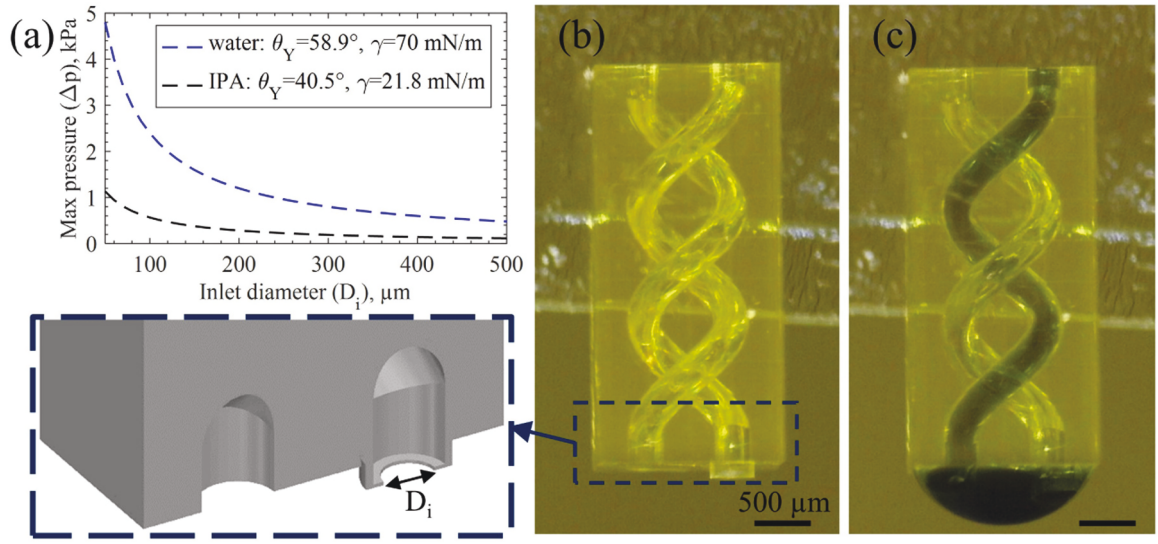

Fig. 12. Hydrophobic inlet design for independent and controllable channel filling (400 μm channel diameter, 300 μm inlet diameter) with (a) maximum liquid pressure that it can withstand, i.e., pressure that needs to be applied to fill the channel with the inlet. A system of helical microchannels (b) before and (c) after immersion in surfactant-free aqueous PEDOT:PSS solution (98.9 wt % water). One of the channels has a hydrophobic inlet preventing the solution from entering the channel.

Conceptualization. **Daewon Kim:** Writing – review & editing, Writing – original draft, Supervision, Resources, Project administration, Funding acquisition, Conceptualization. **Nicholas Reed:** Writing – review & editing, Writing – original draft, Visualization, Validation, Software, Methodology, Investigation, Formal analysis, Data curation, Conceptualization.

Declaration of Competing Interest

The authors declare that they have no known competing financial interests or personal relationships that could have appeared to influence the work reported in this paper.

Data Availability

Data will be made available on request.

Acknowledgments

This material is based upon work supported by the National Science Foundation under Grants No. 2018853 and No. 2229155. The opinions, findings, and conclusions, or recommendations expressed are those of the author(s) and do not necessarily reflect the views of the National Science Foundation.

Appendix A. Supporting information

Supplementary data associated with this article can be found in the online version at doi:10.1016/j.addma.2024.104220.

References

[1] L. Ivy, A. Lal, Solderable multisided metal patterns enables 3D integrable direct laser written polymer MEMS, 35th Int. Conf. Microelectron. Test. Struct. (ICMTS) 2023 (2023) 1–6, https://doi.org/10.1109/ICMTS55420.2023.10094101.
[2] M.A.A. Rehmani, K. Lal, A. Shaukat, K.M. Arif, Laser ablation assisted micropattern screen printed transduction electrodes for sensing applications, Sci. Rep. 12 (1) (2022) 6928, https://doi.org/10.1038/s41598-022-10878-6.
[3] O. Araromi, S. Rosset, H. Shea. Versatile fabrication of PDMS-carbon electrodes for silicone dielectric elastomer transducers, IEEE, 2015, pp. 1905–1908, https://doi.org/10.1109/TRANSDUCERS.2015.7181323.
[4] N.J. Wilkinson, M.A.A. Smith, R.W. Kay, R.A. Harris, A review of aerosol jet printing—a non-traditional hybrid process for micro-manufacturing, Int. J. Adv. Manuf. Technol. 105 (11) (2019) 4599–4619, https://doi.org/10.1007/s00170-019-03438-2.
[5] A. Cohen, M. Kollosche, M. Yuen, D.-Y. Lee, D. Clarke, R. Wood, Batch-sprayed and stamp-transferred electrodes: a new paradigm for scalable fabrication of multilayer dielectric elastomer actuators, Adv. Funct. Mater. 32 (2022) 2205394, https://doi.org/10.1002/adfm.202205394.
[6] M. Corbaci, W. Walter, K. Lamkin-Kennard, Implementation of soft-lithography techniques for fabrication of bio-inspired multi-layer dielectric elastomer actuators with interdigitated mechanically compliant electrodes, Actuators 7 (4) (2018) 73, https://doi.org/10.3390/act7040073.
[7] S. Chatzimichail, P. Supramaniam, O. Ces, A. Salehi-Reyhani, Micropatterning of planar metal electrodes by vacuum filling microfluidic channel geometries, Sci. Rep. 8 (1) (2018) 14380, https://doi.org/10.1038/s41598-018-32706-6.
[8] T. Stark, S. Sikulskyi, R. Srinivasaraghavan Govindarajan, D. Kim, Hydrophilic surface morphology for intricate conductive coatings, SPIE Smart Structures + Nondestructive Evaluation, SPIE, Long Beach, CA, 2023, pp. 10–16, https://doi.org/10.1117/12.2658143.
[9] T. Stark, D. Kim, Electrode filling using capillary action of 3D printed elastomer microchannels, SPIE Smart Structures + Nondestructive Evaluation 12482 (2023) 103–109, https://doi.org/10.1117/12.2658146.
[10] A. Ruggiero, V. Criscuolo, S. Grasselli, U. Bruno, C. Ausilio, C.L. Bovio, O. Bettucci, F. Santoro, Two-photon polymerization lithography enabling the fabrication of PEDOT:PSS 3D structures for bioelectronic applications, Chem. Commun. 58 (70) (2022) 9790–9793, https://doi.org/10.1039/D2CC03152C.
[11] S. Schlatter, G. Grasso, S. Rosset, H. Shea, Inkjet printing of complex soft machines with densely integrated electrostatic actuators, Adv. Intell. Syst. 2 (11) (2020) 2000136, https://doi.org/10.1002/aisy.202000136.
[12] N. Adly, S. Weidlich, S. Seyock, F. Brings, A. Yakushenko, A. Offenhäusser, B. Wolfrum, Printed microelectrode arrays on soft materials: from PDMS to hydrogels, NPJ Flex. Electron. 2 (1) (2018) 15, https://doi.org/10.1038/s41528-018-0027-z.
[13] S. Sikulskyi, S.L. Yu, E. Rojas-Nastrucci, D. Kim, On the electrode-elastomer patterns in dielectric elastomer actuator motion, Proc. of SPIE, Electroactive Polymer Actuators and Devices (EAPAD) XXIII, SPIE 11587 (2021) 287–293, https://doi.org/10.1117/12.2583324.
[14] K. Koch, B. Bhushan, W. Barthlott, Diversity of structure, morphology and wetting of plant surfaces, Soft Matter 4 (10) (2008) 1943–1963, https://doi.org/10.1039/B804854A.
[15] S. Parvate, P. Dixit, S. Chattopadhyay, Superhydrophobic surfaces: insights from theory and experiment, J. Phys. Chem. B 124 (8) (2020) 1323–1360, https://doi.org/10.1021/acs.jpcb.9b08567.
[16] Z. Wang, M. Elimelech, S. Lin, Environmental applications of interfacial materials with special wettability, Environ. Sci. Technol. 50 (2016) 2132–2150, https://doi.org/10.1021/acs.est.5b04351.
[17] X. Ye, Y. Li, Y. Zhang, P. Wang, A comprehensive review: recent developments of biomimetic sensors, J. Bionic. Eng. 19 (4) (2022) 853–876, https://doi.org/10.1007/s42235-022-00181-5.
[18] A. Tuteja, W. Choi, M. Ma, J.M. Mabry, S.A. Mazzella, G.C. Rutledge, G. H. McKinley, R.E. Cohen, Designing superoleophobic surfaces, Science 318 (5856) (2007) 1618–1622, https://doi.org/10.1126/science.1148326.
[19] N.J. Shirtcliffe, G. McHale, M.I. Newton, Learning from superhydrophobic plants: the use of hydrophilic areas on superhydrophobic surfaces for droplet control, Langmuir 25 (24) (2009) 14121–14128, https://doi.org/10.1021/la901557d.

[20] J.M. Wigzell, R.C. Racovita, B.G. Stentiford, M. Wilson, M.T. Harris, I.W. Fletcher, D.P.K. Mosquin, D. Justice, S.K. Beaumont, R. Jetter, J.P.S. Badyal, Smart water channelling through dual wettability by leaves of the bamboo Phyllostachys aurea, Colloids Surf., A 506 (2016) 344–355, https://doi.org/10.1016/j.colsurfa.2016.06.058.
[21] T.L. Liu, C.-J.C. Kim, Turning a surface superrepellent even to completely wetting liquids, Science 346 (6213) (2014) 1096–1100, https://doi.org/10.1126/science.1254787.
[22] E. Arzt, H. Quan, R.M. McMeeking, R. Hensel, Functional surface microstructures inspired by nature – From adhesion and wetting principles to sustainable new devices, Prog. Mater. Sci. 120 (2021) 100823, https://doi.org/10.1016/j.pmatsci.2021.100823.
[23] J. Zhou, D.A. Khodakov, A.V. Ellis, N.H. Voelcker, Surface modification for PDMS-based microfluidic devices, Electrophoresis 33 (1) (2012) 89–104, https://doi.org/10.1002/elps.201100482.
[24] H. Ems, S. Ndao, Microstructure-alone induced transition from hydrophilic to hydrophobic wetting state on silicon, Appl. Surf. Sci. 339 (2015) 137–143, https://doi.org/10.1016/j.apsusc.2015.02.135.
[25] S. Banerjee, D.D. Dionysiou, S.C. Pillai, Self-cleaning applications of TiO2 by photo-induced hydrophilicity and photocatalysis, Appl. Catal., B-Environ. 176-177 (2015) 396–428, https://doi.org/10.1016/j.apcatb.2015.03.058.
[26] E. Gogolides, K. Ellinas, A. Tserepi, Hierarchical micro and nano structured, hydrophilic, superhydrophobic and superoleophobic surfaces incorporated in microfluidics, microarrays and lab on chip microsystems, Microelectron. Eng. 132 (2015) 135–155, https://doi.org/10.1016/j.mee.2014.10.002.
[27] S. Hu, X. Cao, T. Reddyhoff, D. Puhan, S.-C. Vladescu, Q. Wang, X. Shi, Z. Peng, A. J. deMello, D. Dini, Self-compensating liquid-repellent surfaces with stratified morphology, ACS Appl. Mater. Inter. 12 (3) (2020) 4174–4182, https://doi.org/10.1021/acsami.9b22896.
[28] A.D. Lantada, S. Hengsbach, K. Bade, Lotus-on-chip: computer-aided design and 3D direct laser writing of bioinspired surfaces for controlling the wettability of materials and devices, Bioinspir. Biomim. 12 (6) (2017) 066004, https://doi.org/10.1088/1748-3190/aa82e0.
[29] R. Srinivasaraghavan Govindarajan, S. Sikulskyi, Z. Ren, T. Stark, D. Kim, Characterization of photocurable IP-PDMS for soft micro systems fabricated by two-photon polymerization 3D printing, Polymers 15 (22) (2023) 4377, https://doi.org/10.3390/polym15224377.
[30] R. Das, Z. Ahmad, J. Nauruzbayeva, H. Mishra, Biomimetic coating-free superomniphobicity, Sci. Rep. 10 (1) (2020) 7934, https://doi.org/10.1038/s41598-020-64345-1.
[31] X. Liu, H. Gu, M. Wang, X. Du, B. Gao, A. Elbaz, L. Sun, J. Liao, P. Xiao, Z. Gu, 3D printing of bioinspired liquid superrepellent structures, Adv. Mater. 30 (22) (2018) 1800103, https://doi.org/10.1002/adma.201800103.
[32] Y. Lin, R. Zhou, J. Xu, Superhydrophobic surfaces based on fractal and hierarchical microstructures using two-photon polymerization: toward flexible superhydrophobic films, Adv. Mater. Interfaces 5 (21) (2018) 1801126, https://doi.org/10.1002/admi.201801126.
[33] G. Graeber, O.B. Martin Kieliger, T.M. Schutzius, D. Poulikakos, 3D-printed surface architecture enhancing superhydrophobicity and viscous droplet repellency, ACS Appl. Mater. Inter. 10 (49) (2018) 43275–43281, https://doi.org/10.1021/acsami.8b16893.
[34] X. Liu, H. Gu, H. Ding, X. Du, Z. He, L. Sun, J. Liao, P. Xiao, Z. Gu, Programmable liquid adhesion on bio-inspired re-entrant structures, Small 15 (35) (2019) 1902360, https://doi.org/10.1002/smll.201902360.
[35] E. Davis, Y. Liu, L. Jiang, Y. Lu, S. Ndao, Wetting characteristics of 3-dimensional nanostructured fractal surfaces, Appl. Surf. Sci. 392 (2017) 929–935, https://doi.org/10.1016/j.apsusc.2016.09.102.
[36] Z. Dong, M.F. Schumann, M.J. Hokkanen, B. Chang, A. Welle, Q. Zhou, R.H.A. Ras, Z. Xu, M. Wegener, P.A. Levkin, Superoleophobic slippery lubricant-infused surfaces: combining two extremes in the same surface, Adv. Mater. 30 (45) (2018) 1803890, https://doi.org/10.1002/adma.201803890.
[37] S. Hu, X. Cao, T. Reddyhoff, D. Puhan, W. Huang, X. Shi, Z. Peng, D. Dini, Three-dimensional printed surfaces inspired by Bi-gaussian stratified plateaus, ACS Appl. Mater. Inter. 11 (22) (2019) 20528–20534, https://doi.org/10.1021/acsami.9b04020.
[38] Z. Ren, Z. Yang, R. Srinivasaraghavan Govindarajan, F. Madiyar, M. Cheng, D. Kim, Y. Jiang, Two-photon polymerization of butterfly wing scale inspired surfaces with anisotropic wettability, ACS Appl. Mater. Inter. 16 (7) (2024) 9362–9370, https://doi.org/10.1021/acsami.3c14765.
[39] A.-I. Bunea, N. Szczotka, J. Navne, R. Taboryski, Single-step fabrication of superhydrophobic surfaces by two-photon polymerization micro 3D printing, Micro Nano Eng. 19 (2023) 100192–100198, https://doi.org/10.1016/j.mne.2023.100192.
[40] X. Zhao, C. Ma, D.S. Park, S.A. Soper, M.C. Murphy, Air bubble removal: wettability contrast enabled microfluidic interconnects, Sens. Actuat. B-Chem. 361 (2022) 131687, https://doi.org/10.1016/j.snb.2022.131687.
[41] D. Wu, S.-z Wu, Q.-D. Chen, S. Zhao, H. Zhang, J. Jiao, J.A. Piersol, J.-N. Wang, H.-B. Sun, L. Jiang, Facile creation of hierarchical PDMS microstructures with extreme underwater superoleophobicity for anti-oil application in microfluidic channels, Lab Chip 11 (22) (2011) 3873–3879, https://doi.org/10.1039/C1LC20226J.
[42] C.-T. Kung, H. Gao, C.-Y. Lee, Y.-N. Wang, W. Dong, C.-H. Ko, G. Wang, L.-M. Fu, Microfluidic synthesis control technology and its application in drug delivery, bioimaging, biosensing, environmental analysis and cell analysis, Chem. Eng. J. 399 (2020) 125748, https://doi.org/10.1016/j.cej.2020.125748.
[43] S. Sikulskyi, Additively Manufactured Dielectric Elastomer Actuators: Development and Performance Enhancement, Dissertation, Daytona Beach, FL, (2021) 184.
[44] C. Dorrer, J. Rühe, Micro to nano: Surface size scale and superhydrophobicity, Beilstein J. Nanotechnol. 2 (2011) 327–332, https://doi.org/10.3762/bjnano.2.38.
[45] A. Giacomello, L. Schimmele, S. Dietrich, Wetting hysteresis induced by nanodefects, Proc. Natl. Acad. Sci. U. S. A. 113 (3) (2016) E262–E271, https://doi.org/10.1073/pnas.1513942113.
[46] X. Chen, J.A. Weibel, S.V. Garimella, Water and ethanol droplet wetting transition during evaporation on omniphobic surfaces, Sci. Rep. 5 (1) (2015) 17110, https://doi.org/10.1038/srep17110.
[47] R.K. Annavarapu, S. Kim, M. Wang, A.J. Hart, H. Sojoudi, Explaining evaporation-triggered wetting transition using local force balance model and contact line-fraction, Sci. Rep. 9 (1) (2019) 405, https://doi.org/10.1038/s41598-018-37093-6.
[48] D. Zhang, H. Li, X. Chen, H. Qian, X. Li, Effect of surface microstructures on hydrophobicity and barrier property of anticorrosive coatings prepared by soft lithography, Adv. Mater. Sci. Eng. 2014 (2014) 342184, https://doi.org/10.1155/2014/342184.
[49] G. Liu, Y. Liu, M. Zhang, F. Pettersson, M. Toivakka, Fabrication of all-solid organic electrochromic devices on absorptive paper substrates utilizing a simplified lateral architecture, Materials 13 (21) (2020) 4839, https://doi.org/10.3390/ma13214839.